HCl Yield from the OH + ClO Reaction at Temperatures between 218 and 298 K

Jin Jin Wang and Leon F. Keyser*

Atmospheric Chemistry Element, Earth and Space Sciences Division, Jet Propulsion Laboratory, California Institute of Technology, Pasadena, California 91109

Received: February 18, 2001; In Final Form: April 23, 2001

The yield of HCl from the OH + ClO reaction has been determined at 1 Torr total pressure by using the discharge-laminar-flow technique with resonance fluorescence, infrared diode laser spectrometry, and ultraviolet absorption spectrometry detection methods. A known amount of OH is added to a large excess of ClO and the reaction is allowed to go to completion. Under these conditions, the yield is just the ratio of [HCl] produced to initial [OH]. The yield or branching ratio measurement reduces to a measurement of two concentrations; knowledge of the total rate constant or of the branching rate constants is not required. The results are 9.0 ± 4.8% independent of temperature between 218 and 298 K. The errors given are two standard deviations. The results are also independent of the OH source: F + H_2O or H + NO_2. Interference from secondary chemistry is minimized by extrapolating a plot of observed yields to zero initial [OH]. Numerical simulations are used only to check for interference from secondary chemistry and to validate the extrapolation procedure.

Introduction

The reaction of OH with ClO has two exothermic channels (eqs 1a and 1b) which are potentially important in stratospheric chemistry.

$$OH + ClO \rightarrow Cl + HO_2 \quad \Delta H^\circ_{298} = -2.0 \text{ kcal mol}^{-1} \quad (1a)$$

$$OH + ClO \rightarrow HCl + O_2 \quad \Delta H^\circ_{298} = -55.8 \text{ kcal mol}^{-1} \quad (1b)$$

By interconverting HO_x and ClO_x species, reaction 1a affects the relative concentrations of the radical pairs (OH, HO_2) and (ClO, Cl); it also acts as a chain propagation step in the catalytic destruction of O_3:

$$Cl + O_3 \rightarrow ClO + O_2 \quad (2)$$

$$OH + ClO \rightarrow Cl + HO_2 \quad (1a)$$

By converting two radicals that are active in the chain destruction of O_3 into two inactive reservoir species, reaction 1b is a chain termination step. Path 1b is important in the partitioning of odd chlorine species, and, thus, the effect of reaction 1 on stratospheric chemistry depends critically on the branching fraction k_{1b}/k_1.

In the mid to upper stratosphere, models underestimate [HCl] and overestimate [ClO], [HOCl], and [$ClONO_2$]. This results in the predicted [O_3] being lower than observed. A comparison of model results with observed stratospheric concentration profiles shows that the predicted ratios, [HOCl]/[HCl] and [ClO]/[HCl], are higher than the observed values.[1] This study also shows that a 5−10% yield of HCl from OH + ClO with various combinations of a 0−3% yield from HO_2 + ClO (eq 3b) would bring the predicted and observed profiles into much better agreement.

$$HO_2 + ClO \rightarrow HOCl + O_2 \quad (3a)$$

$$HO_2 + ClO \rightarrow HCl + O_3 \quad (3b)$$

Another study has shown that the ratios [ClO]/[HCl] and [$ClONO_2$]/[HCl] are sensitive to a minor HCl channel from the OH + ClO reaction.[2] At 40 km, these ratios are six times more sensitive to reaction 1b with a 7% HCl yield than to reaction 3b with a 3% yield; however, at 30 km reactions 1b and 3b have concentration ratio sensitivities that are large and comparable. A minor yield from reaction 3b would impact Cl partitioning in the mid stratosphere. A study of stratospheric chlorine during the Arctic summer has shown that better agreement between model predictions and measured profiles of HCl and $ClONO_2$ below 35 km are obtained if reaction 1b is included.[3] A recent comparison of observed mixing ratios for ClO, HCl, $ClONO_2$, NO_2, O_3, H_2O, and CH_4 with two atmospheric models is consistent with a 5% yield from reaction 1b.[4]

There have been several measurements of the HCl or DCl yield from reaction 1. Three studies directly detected HCl to obtain k_{1b}/k_1. One study[5] carried out in recent months obtains a value of 6.6 ± 3.5% for the HCl yield. Two earlier studies[6,7] reported 7 ± 3% for HCl production and 5 ± 2% for DCl. All of these results were independent of temperature. Another study[8] detected HCl but reported a yield of 2 ± 12%, not significantly different from zero. Other earlier studies were indirect since they detected changes in OH and/or HO_2 to obtain k_{1a}/k_1 with results ranging from 65% to 88%.[9−11] All of the direct measurements depend on numerical models to extract the yield from observed HCl concentrations; all of the indirect studies, except one, also use models or analyses that depend to some extent on the value of k_1 or other rate constants. Because of the importance of reaction 1 in stratospheric chemistry, the present study was undertaken to further check the reported yields; it was designed to measure HCl concentrations directly and to obtain the yield without reliance on numerical simulations.

* To whom correspondence should be addressed. Fax: (818) 354-5148. E-mail: Leon.F.Keyser@jpl.nasa.gov.

10.1021/jp0106449 CCC: $20.00
Published on Web 06/01/2001

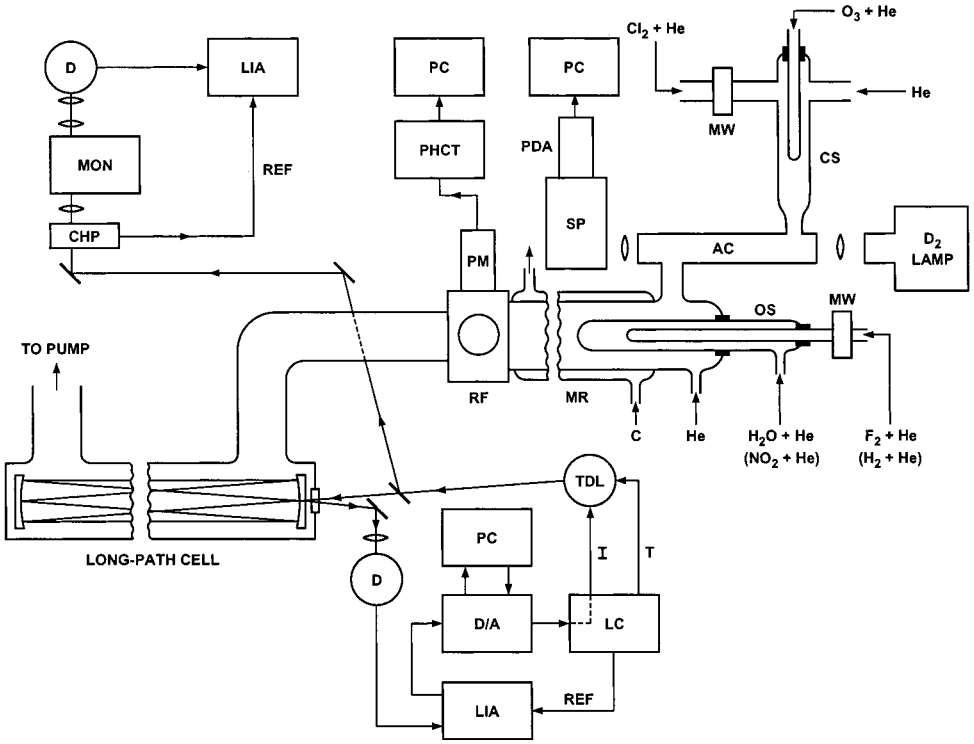

Figure 1. Schematic diagram of the discharge-flow system showing the fixed ClO source, the movable OH source, and the three detection subsystems: resonance fluorescence for OH radicals, UV absorption spectrometry for ClO and O_3, and long-path IR laser absorption for HCl. AC = absorption cell; C = coolant; CHP = mechanical light chopper; CS = ClO source; D = indium antimonide detector; D/A = digital-analogue data acquisition board; I = current control; LC = laser controller; LIA = lock in amplifier; MON = monochromator; MR = main reactor; MW = microwave discharge; OS = OH source; PC = computer; PDA = photodiode array; PHCT = photon counter; PM = photomultiplier; REF = reference signal; RF = resonance fluorescence cell; SP = imaging spectrograph; T = temperature control; TDL = tunable diode laser.

In the present study, a discharge-flow system with resonance fluorescence, infrared diode laser spectrometry, and ultraviolet spectrometry is used to determine the HCl yield or branching fraction, k_{1b}/k_1, between 218 and 298 K. The yield is determined by adding OH to a large excess of ClO and allowing the reaction to go to completion. In the present work, product HCl is observed directly and the accuracy of the measurement depends solely on absolute measurements of the HCl and OH concentrations. Knowledge of the total rate constant or of the branching rate constants is not required. Numerical modeling is used only to assess the importance of secondary chemistry and not to extract the HCl yield.

Experimental Section

The flow system used in the present study has been described recently;[12] so we will discuss in detail only features that are new or critical to the HCl yield measurements. A schematic diagram of the apparatus is shown in Figure 1.

Reactor. The temperature controlled Pyrex main reactor has an internal diameter of 5.04 cm (surface-to-volume ratio, 0.79 cm^{-1}) and is 62 cm in length. At the downstream end, it is connected to a stainless steel resonance fluorescence cell. Pressure is measured by using a 10 Torr capacitance manometer connected to a port between the reactor and the fluorescence cell. At the upstream end are connections to a fixed ClO source and a movable OH source, described in separate sections below. The inner surface of the reactor and outer surface of the movable inlet are coated with halocarbon wax (Series 15−00, Halocarbon Corp.) to minimize wall loss of reactive species. Most of the helium carrier flow bypasses the discharges to minimize production of impurity atoms such as H or O. Total helium flow rates are around 2300 sccm (std atm cm^3 min^{-1}) to establish flow velocities 1150 to 1600 cm s^{-1} at temperatures between 218 and 298 K. The flow system is pumped by a trapped 38 L s^{-1} rotary pump; a throttling valve is used to maintain a total pressure around 1 Torr at the above flow velocities. Temperatures in the reaction zone are maintained within ±2 K by using refrigerated bath circulators (Neslab, ULT-80DD or RTE−110) to pass heat exchange fluids (water or methanol) through the cooling jacket. Temperatures are monitored by two thermocouples (Type E, chromel−constantan) located inside each end of the cooling jacket. Upstream of the main reaction zone, the reactants pass through a pre-cooling region, the length of which depends on the position of the movable source; average lengths are about 50 cm, which gives residence times near 50 ms. This region allows the reactants to cool from room temperature to the main reactor temperature before the reaction starts.

ClO Source. ClO is formed by reacting Cl atoms with an excess of O_3 (eq 2) in a fixed 5.0 cm diameter reactor located upstream of the main reaction zone; all surfaces except the Cl_2 discharge region are coated with halocarbon wax.

$$Cl + O_3 \rightarrow ClO + O_2 \qquad (2)$$

Cl atoms are produced in a 2.45 GHz discharge (50 W) of dilute mixtures of Cl_2 in He; Cl_2 flow rates are between about 0.6 and 1.5 sccm in total flow rates averaging 1440 sccm. Ozone is formed by passing O_2 through a high voltage discharge ozonator (Welsbach model T816) and trapping the O_3 on silica gel at 195 K; the excess O_2 is pumped off and the O_3 is added to the source by passing a stream of He through the cold silica gel trap. In the ClO source, concentrations of ClO and O_3 range from $(0.5-1.2) \times 10^{14}$ and $(0.7-2.2) \times 10^{14}$ molecules cm^{-3}, respectively. Concentrations in the main reactor are lower by factors of 0.38 and 0.28 for main reactor temperatures between

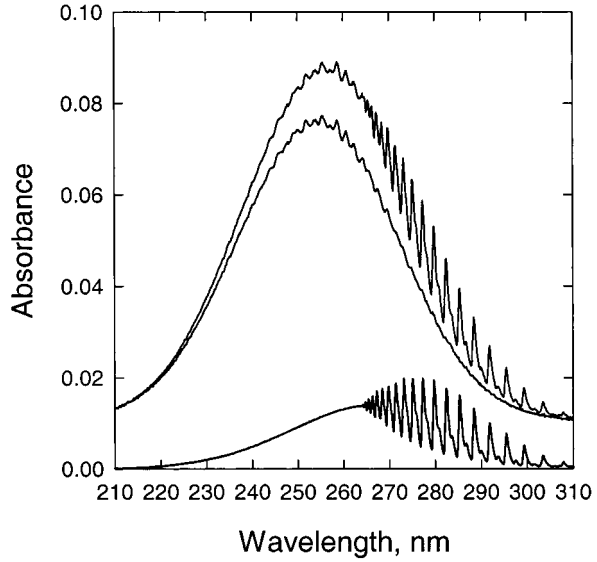

Figure 2. Spectra of ClO and O_3. The upper curve is the observed spectrum of both ClO and O_3; the middle curve is the separated O_3 spectrum after subtraction of ClO, which is shown in the bottom curve. The subtraction technique is discussed in the text. For clarity the top two curves have been displaced upward by 0.01 absorbance units.

218 and 298 K. Total pressure in the source is about 2.2 Torr; the temperature, 298.5 K. At the total flow rate of 1440 sccm, the flow velocity in the source is about 460 cm s^{-1}. The reaction length is 17.5 cm, and this gives a reaction time in the ClO source about 38 ms. Using $k_2 = 1.2 \times 10^{-11}$ cm^3 $molecule^{-1}$ s^{-1},[13] we calculate that the Cl + O_3 reaction is complete in the source even at the lowest O_3 concentrations used. Background HCl from this source is minimized by using research grade Cl_2 (Matheson, 99.999%) and by adding the O_3 to the Cl atoms within a few ms after their formation in the microwave discharge.

ClO and O_3 Determination. After formation in the source reactor, the ClO is passed through a quartz absorption cell 3.0 cm in diameter and 50.1 cm in length; the cell walls, windows, and all connecting tubes downstream are also coated with halocarbon wax. ClO and O_3 are quantitatively determined by using absorption spectrophotometry in the UV region between 210 and 310 nm. The collimated output of a 30 W deuterium lamp (Oriel 60055) passes through the absorption cell and is focused on the entrance slit of a 0.3 m imaging spectrograph (Acton model SP-308); the slit width is set at 20 μm. The absorption spectrum is recorded by using a photodiode array (Oriel model DM220) situated at the exit focal plane of the spectrograph. To avoid any saturation effects, the exposure time is set to 0.25 s, which is at the middle of the linear response region of the diodes under our experimental conditions. A typical spectrum of ClO plus O_3 is shown in Figure 2. Concentrations are determined by using eq 4

$$[M] = A/\sigma_M L \tag{4}$$

where M is ClO or O_3, A is the absorbance defined by eq 5, σ_M is the absorption cross section and L is the absorption path length.

$$A = \ln[(I_o - I_b)/(I_t - I_b)] \tag{5}$$

In eq 5, I_o, I_b, and I_t are the incident, background, and transmitted light intensities, respectively. To determine ClO and O_3 separately, a spectral subtraction method is used; this has been described in detail by Kegley-Owen et al.[14] and will be only summarized here. Three separate spectra are recorded: (1) a ClO reference spectrum with no O_3; (2) an initial O_3 spectrum with no ClO; and (3) the experimental spectrum with both ClO and O_3 present. The reference ClO spectrum is then used to subtract the ClO line structure from the experimental spectrum. This results in two separated spectra for experimental ClO and O_3; typical results are also shown in Figure 2. Although the ClO spectrum in the banded region is used to obtain the separated spectra, the actual concentration of ClO is determined in the continuum region at 253.65 nm where the absorption cross sections are independent of temperature.[15] Ozone is also determined at 253.65 nm; the cross sections used are 4.25×10^{-18} cm^2 $molecule^{-1}$ for ClO[16−19] and 11.58×10^{-18} cm^2 $molecule^{-1}$ for O_3.[20] Production efficiencies based on the fraction of initial Cl_2 converted to ClO are around 75%.

Generally the total flow rates, pressures, and temperatures in the absorption tube differ from those in the main reactor. Therefore, to determine ClO and O_3 concentrations in the main reactor, their concentrations measured in the absorption tube are multiplied by the ratios: $(P_m/P_a)(F_a/F_m)(T_a/T_m)$, where P is the total pressure; F, the total flow rate; and T, the absolute temperature; the subscripts m and a refer to the main reactor and the absorption tube, respectively.

Although we do not need absolute ClO concentrations for the present study, we do need to estimate them as closely as possible to be able to accurately gauge the importance of secondary chemistry. The transit time between the center of the absorption cell where ClO concentrations are determined and the start of the OH + ClO reaction is on average about 75 ms. The main removal mechanisms for ClO are wall loss and self-reaction (eq 6).

$$ClO + ClO \rightarrow Cl_2 + O_2 \tag{6a}$$

$$ClO + ClO \rightarrow 2\,Cl + O_2 \tag{6b}$$

$$ClO + ClO \rightarrow OClO + Cl \tag{6c}$$

$$ClO + ClO + He \rightarrow (ClO)_2 + He \tag{6d}$$

Wall loss of ClO in coated and uncoated Pyrex reactors with surface-to-volume ratios less than about 2 cm^{-1} ranges from less than 0.1 s^{-1} to about 2 s^{-1} even at temperatures as low as 183 K.[8,21,22] Using a wall loss of 1 s^{-1}, we estimate that the loss of ClO due to surface reaction is less than 10%; and at the highest ClO concentrations used, the loss due to self-reaction is about 12%. It should be noted that Cl atoms produced by reactions 6b and 6c will react with excess O_3 in the system to reform ClO; this tends to mitigate the loss due to self-reaction, and the 12% loss given above is really an upper limit. A numerical model (see below) of the ClO source shows that under our conditions only small amounts of ClO dimer, $(ClO)_2$, are formed even at 218 K. At the start of the OH + ClO reaction, calculated $[(ClO)_2]$ is less than 2% of [ClO].

OH Sources. At temperatures between 258 and 298 K, a movable injector is used to produce OH by adding F atoms to an excess of water vapor (eq 7).

$$F + H_2O \rightarrow OH + HF \tag{7}$$

The F atoms are produced in a 2.45 GHz discharge of dilute F_2 in helium. An alumina tube is used for the F_2 discharge, which is operated at a total power of about 20 W. All surfaces except the discharge tube are coated with halocarbon wax. Flow rates of F_2 are 0.01 to 0.8 sccm in a total flow of 660 to 900 sccm.

Water vapor is added by passing a stream of helium through a water bubbler maintained at 18° C. Flow rates of H_2O are determined from the He flow rate, total pressure and the vapor pressure of H_2O. Concentrations of H_2O range over $(1.9-3.5) \times 10^{14}$ molecules cm^{-3}; in the main reactor, concentrations are lower by a factor of about 0.21. The OH source reactor is 1.26 cm in diameter. Total pressure in the source is about 1.4 Torr with flow velocities between 4500 and 5700 cm s^{-1}. The reaction length is set near 15 cm to give reaction times between 2.6 and 3.3 ms. Using $k_7 = 1.4 \times 10^{-11}$ cm^3 $molecule^{-1}$ s^{-1},[21] we calculate that reaction 7 is complete for all of the experimental conditions used. Based on the initial concentrations of F_2 added, reaction efficiencies to form OH are usually between 20 and 30%. This source is used to generate OH concentrations between 1×10^{11} and 6.5×10^{12} molecules cm^{-3} in the main reactor.

At temperatures below 260 K, OH is generated by adding H atoms to an excess of NO_2 (eq 8).

$$H + NO_2 \rightarrow OH + NO \qquad (8)$$

The H atoms are formed in a microwave discharge of dilute mixtures of H_2 in He; a quartz tube is used at powers near 20 W. Again all surfaces except the discharge tube are wax coated. Flow rates of H_2 are 0.032 to 0.42 sccm in a total flow of about 890 sccm. NO_2 is stored as a mixture with O_2. Flow rates are determined by observing the pressure drop in a calibrated volume. In the source, concentrations of NO_2 and O_2 are $(2.2-3.4) \times 10^{13}$ and $(1.8-2.8) \times 10^{13}$ molecules cm^{-3}, respectively; in the main reactor, concentrations are lower by a factor of 0.28. Total pressure in the source is about 1.4 Torr with flow velocities between 5200 and 6200 cm s^{-1}. The reaction length is 5 cm to give a reaction time of about 1 ms. Using $k_8 = 4.0 \times 10^{-10}$ $\exp(-340/T)$ cm^3 $molecule^{-1}$ s^{-1},[21] we estimate that at least 85% of initial H atoms are consumed. Based on initial H_2 concentrations, reaction efficiencies to form OH by reaction 8 are between 25 and 55%. This source is used at temperatures between 218 and 260 K to produce OH at concentrations between 7×10^{11} and 5.5×10^{12} molecules cm^{-3} in the main reactor.

OH Detection. Hydroxyl radicals are detected by resonance fluorescence at a fixed point downstream of the reaction zone. A resonance lamp operated at 50 W of microwave power is used to excite the OH fluorescence. A stream of He saturated with water vapor is passed through the lamp at a total pressure near 4.5 Torr. Hydroxyl radical fluorescence near 308 nm is detected at right angles to the lamp by using an interference filter (Corion 3100-1), photomultiplier tube (EMR 510E), amplifier−discriminator (Ortec 9302), and dual counter−timer (Ortec 994) interfaced to a computer for data acquisition and analysis. The filter used has a transmission of 17% at 308 nm; it is placed between the photomultiplier and a suprasil quartz window that makes the vacuum seal to the flow tube so the filter is never in contact with any of the reagents used. A Corning filter (0−53) is placed in front of the OH lamp to cut off radiation at wavelengths shorter than about 290 nm.

OH Calibration. The accuracy of the HCl yield measurements depends on knowledge of absolute OH concentrations and, thus, on the detection sensitivity of the OH resonance fluorescence lamp. The system is calibrated by generating specific amounts of OH by adding known concentrations of NO_2 to an excess of H atoms (eq 8). H atoms are generated in a fixed microwave discharge (60 W) of dilute mixtures of H_2 in He; this discharge is located just upstream of the main reaction zone and is not shown in Figure 1. NO_2 in He mixtures of specific composition are prepared by using a calibrated capacitance manometer; the mixtures are stored in a 5 L Pyrex flask for later use. A calibrated flow meter is used to add known flows of the NO_2 in He mixture through the movable injector. An example of an OH calibration plot is shown in Figure 3a, where fluorescence intensities are plotted vs reaction length for $[NO_2] = [OH]_o$ about 1.4×10^{12} molecules cm^{-3}. The $[OH]_o$ are corrected for wall loss and for self-reaction (eq 9) by using $k_9 = 4.2 \times 10^{-12}$ $\exp(-240/T)$ cm^3 $molecule^{-1}$ s^{-1}.[21]

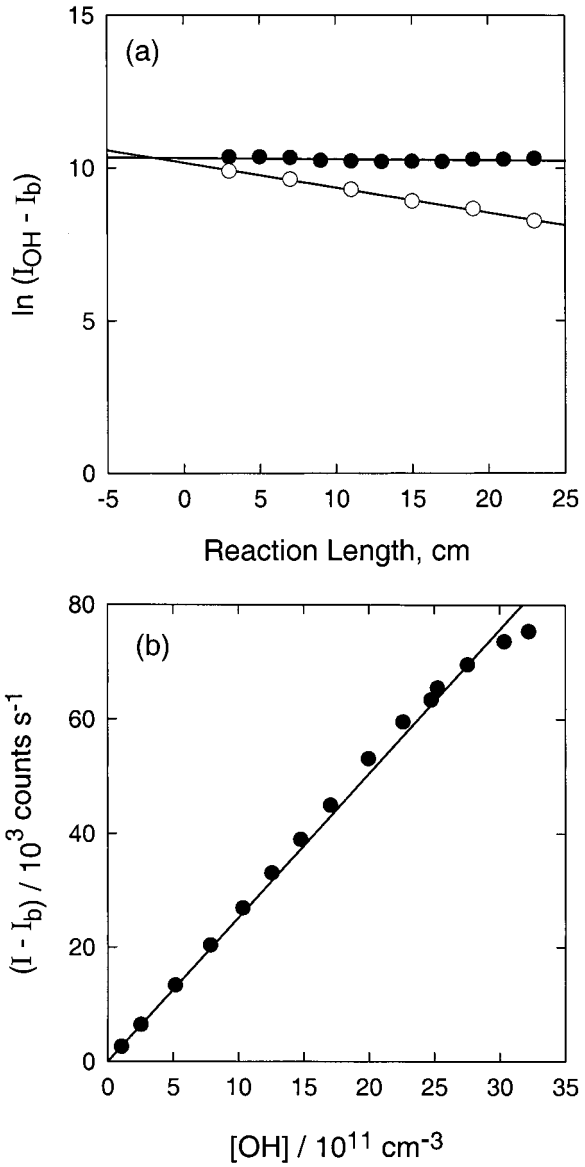

Figure 3. OH calibration plots. Panel (a) is a semilog plot of OH fluorescence intensity vs reaction length. The filled circles are without added propane, the open circles are with added propane; the lines are linear least-squares fits, the intersection of which gives the zero reaction length needed for the corrections described in the text. $[OH] = 1.4 \times 10^{12}$ molecules cm^{-3}. The negative value for zero reaction length occurs because the experimental reference point for measuring reaction length is upstream of the detector position. Panel (b) is a plot of OH fluorescence intensity vs [OH]. The line is a linear least-squares fit; the plot is linear up to about 3×10^{12} molecules cm^{-3}. Possible effects of nonlinearity are discussed in the text.

$$OH + OH \rightarrow O + H_2O \qquad (9)$$

These corrections are made up to the position of the OH detector or zero reaction time, which is determined by the intersection

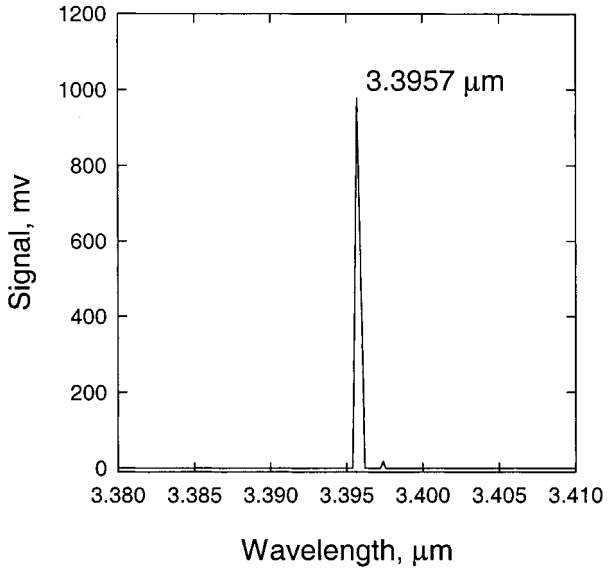

Figure 4. Tunable diode laser output spectrum in the 3.4 μm region showing single mode operation at the HCl R(2) line, 3.3957 μm.

of the OH decay plots with and without added propane. Calibrations are carried out at temperatures used in the yield measurements; no temperature dependence is observed. For the experiment illustrated, intensities are about 3.2×10^4 counts s^{-1}; the lamp sensitivity is then about 2.3×10^{-8} counts s^{-1}/ molecules cm^{-3}. Typically background signals are near 1000 counts s^{-1}; and for the 50 s counting times used, the minimum detectable [OH] is about 3×10^8 molecules cm^{-3} at a signal-to-noise ratio of unity. As seen in Figure 3b, the fluorescence signal is linear with respect to [OH] up to about 3×10^{12} molecules cm^{-3}. Possible effects of nonlinear signals at high [OH] are discussed below.

HCl Detection. Long-path infrared absorption in the region of the fundamental vibration−rotation band near 3.4 μm is used to monitor HCl. A tunable diode laser, TDL, (Laser Components model DH5) is mounted in a liquid nitrogen cooled source dewar (Laser Photonics model L5736). A TDL controller (Laser Photonics model L5830) is used to set the laser temperature, current, and modulation. Several lasers were used in this work; typically they are operated at 84 to 105 K with currents between 300 and 1000 mA to produce output at 2944.9 cm^{-1} coinciding with the R(2) line of $H^{35}Cl$. Indium antimonide detectors (Cincinnati Electronics model SDD-7854-S1 and Kolmar model KISDP-1-J1) with integral preamplifiers are used to monitor the infrared signals; the detectors are operated at 77 K.

To check for multimode operation, the laser output is amplitude modulated at 1100 Hz by using a mechanical light chopper (EG&G model 197) and passed through a 0.5 m focal length monochromator (Acton model SP500). The detector output is demodulated at the reference frequency by using a lock-in amplifier (Stanford Research Systems model SR810). A digital-analog (D/A) data acquisition board (Keithley model DAS-16G) is used to read the lock-in output for computer display and storage. An example of the TDL output spectrum is shown in Figure 4 which confirms that the laser is operating in a single mode at the $H^{35}Cl$ R(2) line frequency.

For absorption measurements, the laser is frequency modulated by superposing a small amplitude current modulation on top of the main laser current; typically a triangular waveform at a frequency of 12.5 kHz and an amplitude of 1.4 mA is used. The D/A board is used to step the laser operating current and thereby scan over a selected spectral range. The combined

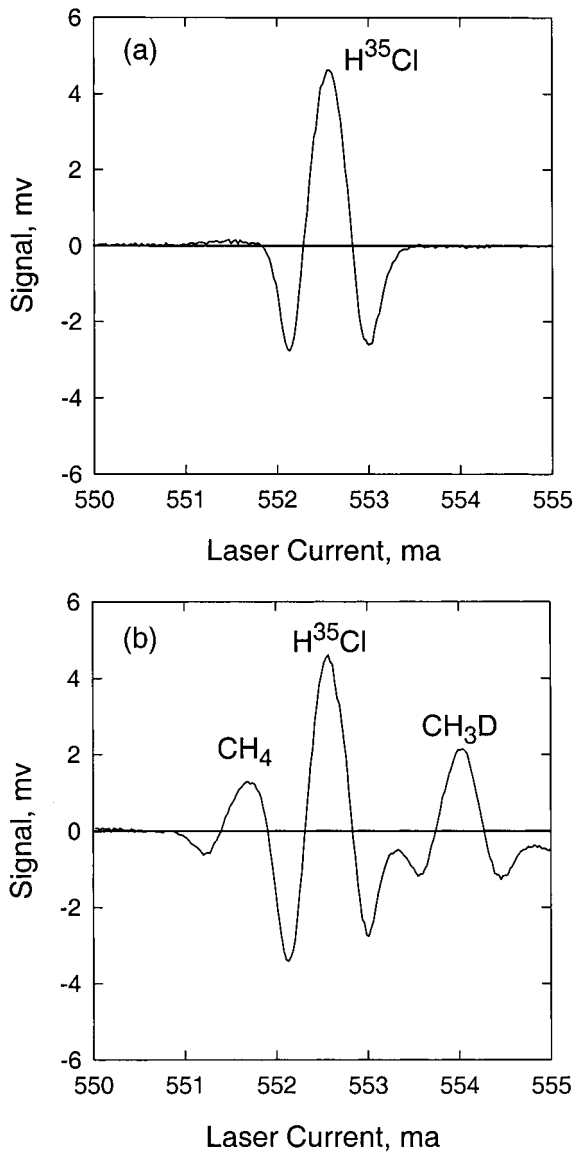

Figure 5. Panel (a) is an HCl absorption signal at the R(2) line, 2944.91 cm^{-1}; the amplitude of the positive peak is taken as the measure of signal strength. Panel (b) displays absorption peaks for an HCl and methane mixture; the methane peaks are CH_4 at 2944.88 cm^{-1} and CH_3D at 2944.96 cm^{-1}. These are used to check for losses of HCl in the system, see text.

resolution of the D/A board and laser controller is 0.0244 mA bit^{-1}. Typical tuning rates of the lasers used range from 0.036 to 0.067 cm^{-1} mA^{-1}, which give spectral step sizes between about 8.8×10^{-4} and 1.6×10^{-3} cm^{-1} bit^{-1}.

The laser signal is passed through a long-path absorption cell (Herriott cell)[23,24] comprising two gold-coated spherical mirrors 7.6 cm in diameter with a focal length of 45.7 cm. The mirrors are positioned 84.6 cm apart to give 42 passes and a total absorption path length of 35.5 m. A Pyrex housing encloses the cell and is provided with connections to the flow reactor and pumping system. After exiting the long-pass cell, the modulated laser beam is directed to a detector-preamplifier, the output of which is sent to a lock-in amplifier (SRS model SR830) where it is demodulated at the first harmonic frequency, 2f, or in this case 25 kHz. The resulting "second derivative" absorption signal is acquired by using the D/A board and then displayed and stored in a computer system. An example of an HCl signal is shown in Figure 5a. The amplitude of the positive peak is taken as a measure of HCl signal strength.

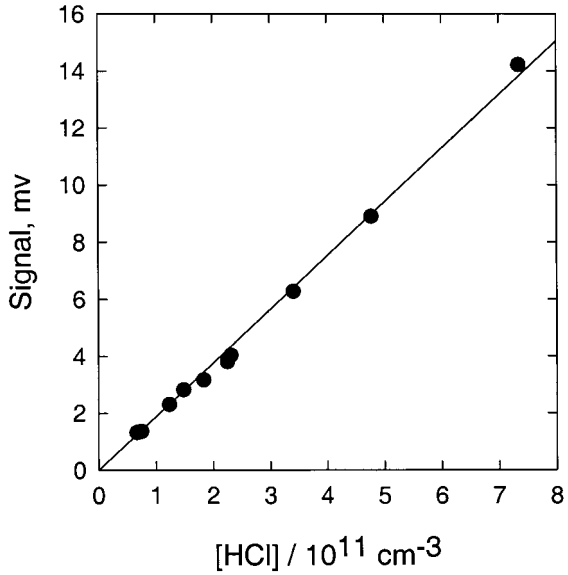

Figure 6. Calibration plot of HCl signal vs [HCl].

HCl Calibration. HCl detection sensitivity is calibrated by adding known amounts of HCl to the absorption cell under conditions of pressure and temperature similar to those used for the actual product yields. HCl in He mixtures of known composition are prepared using a calibrated capacitance manometer and then stored in a Pyrex 5 L flask. Except for a stainless steel flow meter, all connecting lines and valves in the system between the storage flask and the reactor are Pyrex or Teflon to minimize surface loss of HCl. Known flows of the HCl in He mixture are added just upstream of the main reactor. The flow rate is read before the HCl signal is recorded and again afterward; the average of the two readings is used. During the actual HCl signal intensity measurement, the flow meter is bypassed. Because sensitivities depend on the specific laser used, the laser operating conditions, the absorption path length, and the optical alignment, calibrations are carried out as part of each HCl yield experiment. Signals are recorded at various [HCl] and an example of the resulting calibration plot is shown in Figure 6. The signal is linear up to at least [HCl] $\approx 8 \times 10^{11}$ cm^{-3}. Observed sensitivities range from about 2.0×10^{-11} to 3.5×10^{-9} mV cm^3 $molecule^{-1}$. At the lowest sensitivity, the detection limit at a signal-to-noise ratio of unity is about 5×10^9 molecules cm^{-3}.

In separate experiments, the HCl calibrations are checked for possible losses by simultaneously adding known amounts of CH_4; a typical spectrum with both HCl and CH_4 present is shown in Figure 5b. By using literature values for the line strengths of HCl and CH_4 at 295 K,[25] the known concentration of CH_4 obtained from flow measurements, and the observed signal intensities, we are able to calculate the HCl concentration (eq 10).

$$[\mathrm{HCl}] = (\sigma_{\mathrm{methane}}/\sigma_{\mathrm{HCl}})\,(\mathrm{signal}_{\mathrm{HCl}}/\mathrm{signal}_{\mathrm{methane}})\,[\mathrm{CH_4}] \quad (10a)$$

$$(\sigma_{\mathrm{methane}}/\sigma_{\mathrm{HCl}}) = (S_{\mathrm{methane}}/S_{\mathrm{HCl}})\,(\nu_{\mathrm{HCl}}/\nu_{\mathrm{methane}})(M_{\mathrm{methane}}/M_{\mathrm{HCl}})^{1/2} \quad (10b)$$

Two methane lines that bracket the HCl R(2) line at 2944.91 cm^{-1} are used: CH_4 at 2944.88 cm^{-1} and CH_3D at 2944.96 cm^{-1} with respective line strengths of 5.695×10^{-24} and 9.200×10^{-24} cm $molecule^{-1}$. The HCl line strength used is 5.044×10^{-19} cm $molecule^{-1}$. In eq 10, σ is the absorption cross-section; S, the line strength; ν, the line frequency, and M, the molecular weight. No significant differences are found in the concentrations of HCl calculated from eq 10 and those calculated from the added HCl flow rates; this demonstrates that no significant HCl losses are occurring between the main reactor and the long-path cell.

Meter Calibrations. Three mass flow measurements are crucial in determining the absolute concentrations of OH and HCl needed in the present study: the total flow of He, the flow of HCl, and the flow of NO_2, which is converted to OH (see above). These flow meters are calibrated directly for He by using the volume change at constant pressure (bubble meter) method or by the pressure rise at constant volume method. Since the mole fractions of HCl and NO_2 in He are less than a few percent, the flow of these gases is determined by the flow of He and their mole fractions. Other less critical flow meters are calibrated by reference to these flow meters. Pressure gauges are calibrated by using an oil manometer. All thermocouples used in the experiments are calibrated at 273 and near 195 K by using ice plus water and CO_2 plus methanol baths, respectively. Barometric corrections are used to obtain the CO_2 equilibrium temperature. The temperature in the reaction zone is measured by using a thermocouple probe in place of the movable inlet. At low temperatures the probe reading is 1 to 2 K lower than the two thermocouples in the cooling jacket, while at 298 K the probe temperature is within 0.2 K. All temperatures reported are based on the probe readings.

Reagents. Several gases used are research grade (99.9999%): He, CH_4, and H_2. Other gases are research grade Cl_2 (99.999%), ULSI grade HCl (99.999%), ultrahigh purity O_2 (99.8%), 0.5% to 5% mixtures of F_2 in He, CP grade NO (99% min), and instrument grade propane (99.5% min). As described above (see ClO source), O_3 is formed by passing O_2 through a high voltage discharge. NO_2 for OH calibrations is prepared from NO by adding an excess of O_2 and letting the mixture stand overnight. The excess O_2 is removed by pumping the mixture through a trap at 195 K where the NO_2 condenses as a white solid; then mixtures are prepared by warming the solid and allowing the NO_2 gas to expand into a 5 L flask to which He is then added. NO_2 for use in the OH source is produced by adding an excess of O_2 to NO and stored in a thermally insulated Pyrex flask of known volume (4821 cm^3). The main carrier He is further purified by passage through a molecular sieve (Linde 3A) trap at 77 K just prior to use.

Results

HCl Yields. To obtain the HCl yield from reaction 1, we measure the amount of HCl produced for a given amount of OH reacted. We can write the rates of OH loss and HCl formation (eqs 11 and 12).

$$-\mathrm{d[OH]}/\mathrm{d}t = k_1[\mathrm{ClO}]\,[\mathrm{OH}] \quad (11)$$

$$\mathrm{d[HCl]}/\mathrm{d}t = k_{1b}[\mathrm{ClO}][\mathrm{OH}] \quad (12)$$

Integrating these equations from time zero to some time, t, we have

$$k_{1b}/k_1 = ([\mathrm{HCl}]_t/[\mathrm{OH}]_o)\{1 - \exp(-k_1[\mathrm{ClO}]t)\}^{-1} \quad (13)$$

At large t, this becomes

$$k_{1b}/k_1 = ([\mathrm{HCl}]_\infty/[\mathrm{OH}]_o) \quad (14)$$

where $[OH]_o$ is the initial OH concentration and $[HCl]_\infty$ is the HCl concentration at reactions times such that at least 98% of

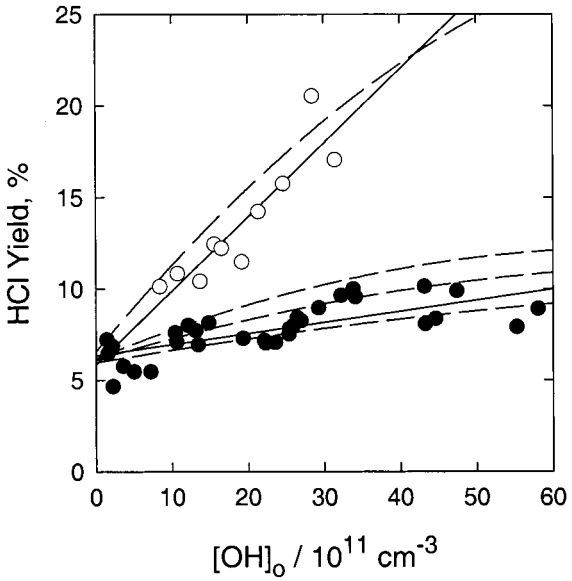

Figure 7. HCl yield vs $[OH]_o$. The filled circles are data taken at 298 K; the open circles are data at 218 K. The solid lines through the data are linear least-squares fits; the dashed lines are HCl yields calculated from a numerical model, see text for details.

the initial OH is consumed. The branching ratio measurement thus reduces to a measurement of two concentrations.

The HCl product determinations are done by measuring the initial OH signal with the ClO off; then ClO is added and the HCl signal is recorded. Background HCl signals are determined at the start and end of each run by turning off the OH; the average is then subtracted from the total HCl signal. Calibrated sensitivities are then used to convert the observed OH and HCl signals to absolute concentrations and, thus, determine the branching ratio or HCl yield by using eq 14. The system HCl background signal without added ClO is less than about 5×10^9 cm^{-3}. During the yield measurements with ClO added, the HCl background generally varies only slightly; typical values are $(5-8) \times 10^{10}$ cm^{-3}. Observed HCl concentrations from OH + ClO range from about 8×10^9 to 1×10^{12} molecules cm^{-3} and depend on the initial OH concentrations.

No corrections are needed for viscous pressure drop or for diffusion. However, the initial OH concentrations are corrected for losses by self-reaction (eq 9) and by reaction at the walls between the OH source exit and the OH detection point. Average corrections range from about 10% to 75%, with most below 30%. The initial ClO concentrations and the reaction lengths are set such that OH is reduced to less than 2% of its initial value within the constant temperature region of the main reactor.

At each temperature HCl yields are plotted vs $[OH]_o$; example plots at the two extreme temperatures studied are shown in Figure 7. The increase in yield at higher $[OH]_o$ is due to HCl production from secondary reactions such as Cl + HO_2 (eq 15a); this is discussed below in the computer simulations section.

$$Cl + HO_2 \rightarrow HCl + O_2 \qquad (15a)$$

$$Cl + HO_2 \rightarrow ClO + OH \qquad (15b)$$

The best estimate of the yield free of secondary chemistry can be obtained by extrapolating the data to zero $[OH]_o$. The model results (discussed below) show some negative curvature as $[OH]_o$ increases; this is most likely due to secondary HCl losses at high radical concentrations. To fit our experimental data we can use a quadratic expression with the constraint that the quadratic coefficient be less than or equal to zero in order to have the same form as the model results. We can also fit our data using a linear equation with no significant difference in the results. We report here the linear fit and obtain HCl yields by extrapolating a least-squares fit of the data to zero $[OH]_o$. The yields obtained in this way are summarized in Table 1 and Figure 8. The errors are twice the standard deviation obtained from the linear least-squares analyses of the HCl yield vs $[OH]_o$ plots. There is no significant dependence on temperature between 218 and 298 K. The overall average of 15 runs is (9.0 ± 4.8)%, where the errors are at the 95% confidence level. Sources of the observed scatter can be analyzed by considering that the yield is obtained from a ratio of OH to HCl detector calibrations and a ratio of HCl to OH signal strengths. We estimate that the sum of systematic and random errors in calibrating the detector sensitivities are about ± 25% for each detector. Combining these we obtain a ±35% uncertainty in the calibration ratio. This uncertainty becomes part of the observed statistical uncertainty because each yield measurement uses a different calibration ratio. The statistical errors also include random errors in the OH and HCl signal readings, which we estimate to be about ±10%; when these are combined with calibration errors, the error estimate becomes about ±40%, which is close to the observed scatter. Systematic errors in flow meter and pressure gauge calibrations, estimated at 3% and 2%, respectively, are not added to the statistical error because they tend to cancel in a ratio measurement.

TABLE 1: Summary of Observed HCl Yields from OH + ClO[a,b]

T (K)	$[ClO]$[c]	$[O_3]$[c]	$[OH]_o$[d]	yield, %[e]
298.0	2.56	1.88	1.1−31	7.7 ± 1.0
297.4	1.53	4.03	5.0−38	4.3 ± 2.8
297.4	1.75	3.92	1.4−58	6.3 ± 0.6
297.0	2.28	2.76	2.2−38	9.7 ± 0.6
287.5	1.40	3.67	1.5−44	8.6 ± 1.0
278.0	1.96	2.57	9.7−35	12.8 ± 5.2
277.8	1.95	1.89	1.8−42	9.2 ± 1.0
277.8	1.73	3.39	2.2−50	8.2 ± 1.2
268.0	3.07	2.86	1.6−57	9.1 ± 0.8
263.0	2.90	2.29	1.9−56	9.1 ± 1.2
259.8[f]	3.05	2.93	8.4−48	13.2 ± 3.0
257.8	2.45	2.33	1.6−65	11.4 ± 0.4
241.4[f]	3.20	6.22	7.0−54	10.0 ± 1.8
226.0[f]	3.34	2.94	9.3−41	9.5 ± 4.6
217.8[f]	3.19	4.70	8.4−32	5.8 ± 2.8

[a] All concentrations are in the main reactor. [b] Unless indicated otherwise OH source was F + H_2O. [c] Units are 10^{13} molecules cm^{-3}. [d] Units are 10^{11} molecules cm^{-3}. [e] Errors are two standard deviations. [f] OH source was H + NO_2.

OH Wall Loss. The rate of OH loss on the main reactor walls is needed to correct the initial OH concentrations used to determine HCl yields. The wall loss is measured by adding F atoms to an excess of H_2O or H atoms to an excess of NO_2 at various reaction lengths. A plot of OH fluorescence signal vs reaction length is extrapolated to zero reaction time to determine the initial fluorescence signal. This initial signal is converted to an initial OH concentration by using the calibrated lamp sensitivity. The OH wall loss is determined as the remaining loss after correcting for reaction 9. What is called OH wall loss here is actually the sum of all background losses of OH. The results are summarized in Table 2. At room-temperature, wall losses averaged about 8 to 11 s^{-1}; at lower temperatures losses increased slightly to about 16 s^{-1} at 258 K. At temperatures below 258 K, the $[OH]_o$ is measured at room-temperature just downstream of the main reactor; for these yield measurements the $[OH]_o$ is corrected by using the 297 K wall loss.

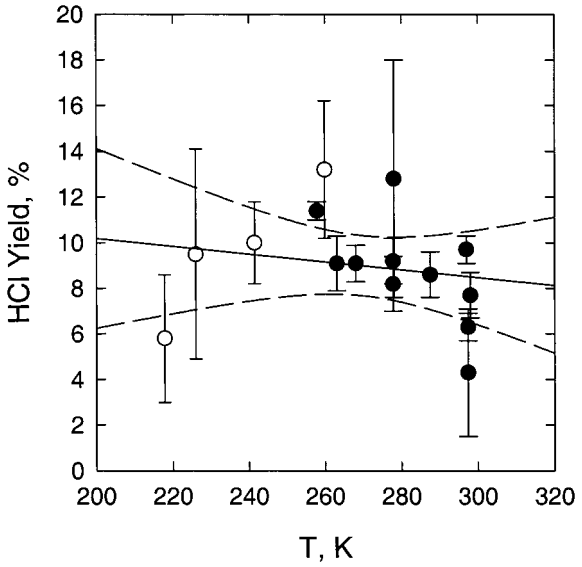

Figure 8. HCl yield vs temperature. Filled circles represent experiments for which the OH source was $F + H_2O$; open circles, OH source was $H + NO_2$. Error bars are two standard deviations. Solid line is linear least-squares fit to the data; dashed lines show the 95% confidence interval.

TABLE 2: OH Wall Loss[a]

OH source	T, K	k_{wall}, s^{-1}
$H + NO_2$	297.1	8.6
	297.0	8.6
	297.0	15.2
		av = 10.8 ± 3.8
$F + H_2O$	296.9	8.4
	297.2	7.2
		av = 7.8 ± 0.8
$F + H_2O$	285.2	8.7
	278.1	9.6
	268.2	13.1
	262.8	17.0
	257.9	15.9

[a] Errors are one standard deviation.

Discussion

Computer Simulations and Secondary Chemistry. Numerical models were used to check for possible interference from secondary chemistry and to verify the extrapolation procedure used to obtain the HCl yields in this study. The modeling was not used to obtain any yield data, which are calculated solely from observed concentration ratios, eq 14. The simulations were carried out using a differential equation integrator, CHEMRXN, which is based on standard Gear algorithms. CHEMRXN has been validated[12] by comparison with two other programs: ACUCHEM,[26] which is also a Gear routine, and CKS,[27] which is based on a stochastic algorithm. Concentrations and reaction times were close to those actually used in the experimental runs. Each radical source was modeled separately and then combined to model the OH + ClO reaction system; the reactions and rate constants used are listed in Table 3. At 298 K, the $F + H_2O$ reaction (eq 7) was used as the OH source in the model; at 218 K the $H + NO_2$ reaction (eq 8) was used. To check the validity of the extrapolation procedure, several concentrations of OH were combined with excess ClO in the model. The production of HCl was followed for 115 ms in order to simulate the time between the start of OH + ClO and HCl detection at the center of the long-pass cell.

An example of the model output at 298 K is shown in Figure 9. The model HCl yield is taken as the ratio of [HCl] at 115 ms

TABLE 3: Reactions Used in Numerical Simulations

reaction	rate constant[a]	refs
$ClO + OH \rightarrow Cl + HO_2$	$0.94^b \times [7.4 \times 10^{-12} \exp(+270/T)]$	13
$ClO + OH \rightarrow HCl + O_2$	$0.06^b \times [7.4 \times 10^{-12} \exp(+270/T)]$	13
$Cl + HO_2 \rightarrow HCl + O_2$	$1.8 \times 10^{-11} \exp(+170/T)$	21
$Cl + HO_2 \rightarrow ClO + OH$	$4.1 \times 10^{-11} \exp(-450/T)$	21
$ClO + HO_2 \rightarrow HOCl + O_2$	$4.8 \times 10^{-13} \exp(+700/T)$	21
$ClO + ClO \rightarrow OClO + Cl$	$3.5 \times 10^{-13} \exp(-1370/T)$	21
$ClO + ClO \rightarrow 2\ Cl + O_2$	$3.0 \times 10^{-11} \exp(-2450/T)$	21
$ClO + ClO \rightarrow Cl_2 + O_2$	$1.0 \times 10^{-12} \exp(-1590/T)$	21
$ClO + ClO + He \rightarrow (ClO)_2 + He$	$2.2 \times 10^{-32} (T/298)^{-3.10}$	21
$OH + OH \rightarrow O + H_2O$	$4.2 \times 10^{-12} \exp(-240/T)$	21
$HO_2 + HO_2 \rightarrow H_2O_2 + O_2$	$2.3 \times 10^{-13} \exp(+600/T)$	21
$OH + HO_2 \rightarrow H_2O + O_2$	$4.8 \times 10^{-11} \exp(+250/T)$	13
$OH + O_3 \rightarrow HO_2 + O_2$	$1.5 \times 10^{-12} \exp(-880/T)$	13
$HO_2 + O_3 \rightarrow OH + 2\ O_2$	$2.0 \times 10^{-14} \exp(-680/T)$	13
$OH + HCl \rightarrow Cl + H_2O$	$2.6 \times 10^{-12} \exp(-350/T)$	13
$Cl + O_3 \rightarrow ClO + O_2$	$2.3 \times 10^{-11} \exp(-200/T)$	13
$OH + Cl_2 \rightarrow HOCl + Cl$	$1.4 \times 10^{-12} \exp(-900/T)$	21
$OH + Cl \rightarrow HCl + O$	$9.8 \times 10^{-12} \exp(-2860/T)$	28
$O + ClO \rightarrow Cl + O_2$	$3.0 \times 10^{-11} \exp(+70/T)$	13
$O + HO_2 \rightarrow OH + O_2$	$3.0 \times 10^{-11} \exp(+200/T)$	13
$H + HO_2 \rightarrow 2\ OH$	7.8×10^{-11}	21
$H + HO_2 \rightarrow O + H_2O$	2.0×10^{-12}	21
$H + HO_2 \rightarrow H_2 + O_2$	7.0×10^{-12}	21
$Cl + HOCl \rightarrow Cl_2 + OH$	3.8×10^{-13}	28
$Cl + HOCl \rightarrow HCl + ClO$	1.2×10^{-12}	28
$Cl + H_2O_2 \rightarrow HCl + HO_2$	$1.1 \times 10^{-11} \exp(-980/T)$	21
$Cl + OClO \rightarrow 2\ ClO$	$3.4 \times 10^{-11} \exp(+160/T)$	21
$O + O_3 \rightarrow 2\ O_2$	$8.0 \times 10^{-12} \exp(-2060/T)$	21
$H + O_3 \rightarrow OH + O_2$	$1.4 \times 10^{-10} \exp(-470/T)$	21
$OH + HOCl \rightarrow H_2O + ClO$	$3.0 \times 10^{-12} \exp(-500/T)$	21
$O + HOCl \rightarrow OH + ClO$	1.7×10^{-13}	21
$H + HOCl \rightarrow HCl + OH$	6.7×10^{-13}	28
$H + HOCl \rightarrow H_2 + ClO$	3.6×10^{-12}	28
$O + HCl \rightarrow OH + Cl$	$1.0 \times 10^{-11} \exp(-3300/T)$	21
$H + HCl \rightarrow H_2 + Cl$	$1.3 \times 10^{-11} \exp(-1710/T)$	28
$OH + H_2O_2 \rightarrow HO_2 + H_2O$	$2.9 \times 10^{-12} \exp(-160/T)$	21
$O + OH \rightarrow H + O_2$	$2.2 \times 10^{-11} \exp(+120/T)$	21
$OH + OClO \rightarrow HOCl + O_2$	$4.5 \times 10^{-13} \exp(+800/T)$	21
$O + H_2O_2 \rightarrow OH + HO_2$	$1.4 \times 10^{-12} \exp(-2000/T)$	21
$H + H_2O_2 \rightarrow H_2 + HO_2$	$2.8 \times 10^{-12} \exp(-1890/T)$	28
$H + H_2O_2 \rightarrow OH + H_2O$	$1.7 \times 10^{-11} \exp(-1800/T)$	28
$O + OClO \rightarrow ClO + O_2$	$2.4 \times 10^{-12} \exp(-960/T)$	21
$H + Cl_2 \rightarrow HCl + Cl$	$1.4 \times 10^{-10} \exp(-590/T)$	28
$F + H_2O \rightarrow OH + HF$	1.4×10^{-11}	21
$F + HO_2 \rightarrow HF + O_2$	8.3×10^{-11}	28
$F + O_3 \rightarrow FO + O_2$	$2.2 \times 10^{-11} \exp(-230/T)$	21
$F + HOCl \rightarrow$ Products	3.7×10^{-11}	28
$F + HOCl \rightarrow ClF + OH$	1.2×10^{-11}	28
$F + HCl \rightarrow Cl + HF$	1.2×10^{-11}	28
$F + H_2O_2 \rightarrow HO_2 + HF$	5.0×10^{-11}	28
$F + Cl_2 \rightarrow ClF + Cl$	1.2×10^{-10}	28
$O + F_2 \rightarrow FO + F$	1.0×10^{-16}	28
$H + F_2 \rightarrow HF + F$	$1.4 \times 10^{-11} \exp(-670/T)$	28
$O + FO \rightarrow F + O_2$	2.7×10^{-11}	21
$H + FO \rightarrow F + OH$	1.6×10^{-11}	28
$H + FO \rightarrow O + HF$	8.2×10^{-12}	28
$FO + FO \rightarrow 2\ F + O_2$	1.0×10^{-11}	21
$ClO + NO_2 + He \rightarrow ClONO_2 + He$	$2.7 \times 10^{-33} \exp(+1110/T)$	28
$ClO + NO \rightarrow Cl + NO_2$	$6.4 \times 10^{-12} \exp(+290/T)$	21
$OH + H_2 \rightarrow H + H_2O$	$5.5 \times 10^{-12} \exp(-2000/T)$	21
$OH + NO_2 + He \rightarrow HNO_3 + He$	$1.0 \times 10^{-30} (T/298)^{-2.90}$	28
$OH + NO + He \rightarrow HNO_2 + He$	$1.8 \times 10^{-32} \exp(+855/T)$	28
$OH + HNO_3 \rightarrow H_2O + NO_3$	$8.3 \times 10^{-13} \exp(+850/T)$	28
$HO_2 + NO_2 + He \rightarrow HO_2NO_2 + He$	$6.0 \times 10^{-32} (T/298)^{-3.20}$	28
$HO_2 + NO \rightarrow OH + NO_2$	$3.5 \times 10^{-12} \exp(+250/T)$	21
$Cl + H_2 \rightarrow H + HCl$	$3.7 \times 10^{-11} \exp(-2300/T)$	21
$Cl + NO_2 + He \rightarrow ClONO + He$	$1.3 \times 10^{-30} (T/298)^{-2.00}$	21
$Cl + NO + He \rightarrow NOCl + He$	$6.9 \times 10^{-33} \exp(+530/T)$	28
$H + NO_2 \rightarrow OH + NO$	$4.0 \times 10^{-10} \exp(-340/T)$	21
$H + NO + He \rightarrow HNO + He$	$1.7 \times 10^{-32} \exp(+270/T)$	28
$O + NO_2 \rightarrow NO + O_2$	$5.6 \times 10^{-12} \exp(+180/T)$	13
$O + NO + He \rightarrow NO_2 + He$	$2.3 \times 10^{-32} \exp(+290/T)$	28
$NO + O_3 \rightarrow NO_2 + O_2$	$3.0 \times 10^{-12} \exp(-1500/T)$	13
$Cl + (ClO)_2 \rightarrow Cl_2 + Cl + O_2$	1.0×10^{-10}	21
$OH + (ClO)_2 \rightarrow HOCl + Cl + O_2$	5.0×10^{-11}	est
$O + (ClO)_2 \rightarrow ClO + Cl + O_2$	5.0×10^{-11}	est
$H + (ClO)_2 \rightarrow HCl + Cl + O_2$	5.0×10^{-11}	est
$O + Cl_2 \rightarrow Cl + ClO$	$7.4 \times 10^{-12} \exp(-1650/T)$	28
$OH + ClONO_2 \rightarrow$ products	$1.2 \times 10^{-12} \exp(-330/T)$	21
$Cl + ClONO_2 \rightarrow Cl_2 + NO_3$	$6.5 \times 10^{-12} \exp(+135/T)$	21
$OH +$ wall $\rightarrow$ products	10	meas
$Cl +$ wall $\rightarrow$ products	5	est

[a] Units are cm^6 $molecule^{-2}$ s^{-1}, cm^3 $molecule^{-1}$ s^{-1}, and s^{-1} for third, second and first-order reactions, respectively. [b] Branching ratio varies in models.

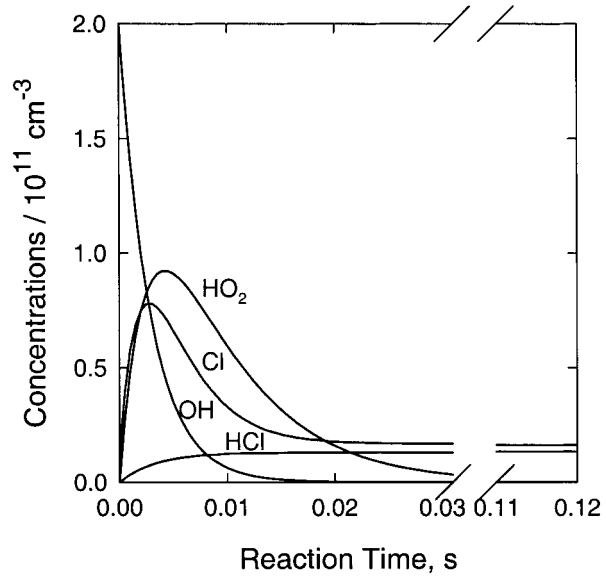

Figure 9. Output from a numerical model simulating the OH + ClO reaction system at 298 K; $[OH]_o = 2.0 \times 10^{11}$, $[ClO] = 1.8 \times 10^{13}$, $[O_3] = 3.0 \times 10^{13}$ molecules cm^{-3}. Models are used only to check for effects of secondary chemistry on the observed HCl yields.

to $[OH]_o$. As shown in the figure, removal of OH occurs in less than 10−15 ms; this ensures that the HCl production occurs in the temperature controlled main reactor. HO_2 and Cl atoms are produced by reaction 1a. Cl atoms are removed mainly by reaction with O_3 (eq 2) but also by reaction with HO_2 (eq 15). HO_2 is removed mainly by reaction with ClO (eq 3).

Model results are compared with experiment in Figure 7 where the filled circles are experimental yields near 298 K, the open circles are experimental yields near 218 K, and the dashed lines give the modeled HCl yields as a function of $[OH]_o$. Because product $[HO_2]$ from reaction 1 is proportional to $[OH]_o$, the observed increase in yield at higher $[OH]_o$ is most likely due to the increasing importance of HCl production from reactions of HO_2 such as ClO + HO_2 (eq 3b) and Cl + HO_2 (eq 15a).

Several studies of reaction 3 agree that, at pressures below 10 Torr, the HCl yield is less than 1−2%.[29−33] One study at 210 K and 700 Torr of argon and oxygen found an HCl yield of (5 ± 2)% from ClO + HO_2.[30] Because the observed yields from reaction 3 at low pressures are somewhat uncertain and are less than the experimental uncertainties in this study, no corrections have been made for possible HCl production from this reaction.

Several studies of Cl + HO_2 (eq 15) have found high HCl yields;[34−36] the currently accepted values are 78% and 88% at 298 and 218 K, respectively.[21] The middle dashed line near the 298 K data is for a 78% yield from reaction 15a and the agreement with the observed dependence on $[OH]_o$ is reasonably good. Better agreement can be obtained if the yield from 15a is set to 50%, at which point the model line (lowest dashed line) is almost indistinguishable from the linear least-squares fit in Figure 7. The upper line near the 298 K data is for a 100% yield, which is clearly too high. Extrapolating the model line for 78% HCl yield from Cl + HO_2 to zero $[OH]_o$ gives an intercept of 6.2%, which agrees within 5% with the input HCl yield of 6.0% from OH + ClO used in the model. The dashed line near the 218 K data is the model result using an 88% yield of HCl from reaction 15. The model correctly predicts the observed greater sensitivity to $[OH]_o$; the extrapolated model yield agrees within 10% with the input value. As a check of the extrapolation, the HCl yield from reaction 1 was set to zero; this leaves reaction 15a as the only major source of HCl in the model. When the model results are extrapolated to zero $[OH]_o$, the intercepts are less than 0.6%; this shows that the extrapolation removes essentially all interference from reaction 15a.

The model results show that at high $[OH]_o$ some interference from HCl produced by Cl + HO_2 is occurring but by extrapolating to zero $[OH]_o$ this interference can be eliminated. The higher sensitivity at 218 K is most likely due to the presence of NO, which is generated along with OH by the source reaction, H + NO_2 (eq 8). The NO reacts with the excess ClO (eq 16) to produce Cl atoms, some of which react with HO_2 (eq 15a) to produce additional HCl.

$$ClO + NO \rightarrow Cl + NO_2 \qquad (16)$$

Comparison with Earlier Results. HCl yield measurements from OH + ClO are summarized in Table 4 where the error limits are as given in the original papers; they generally are at the 95% confidence level and include estimates of systematic uncertainties. A variety of experimental techniques have been used, but only the last five entries in the table have looked directly for HCl product. Tyndall et al.[5] used tunable diode laser infrared spectrometry to monitor HCl production following the flash photolysis of $Cl_2-O_3-O_2-H_2O$ mixtures in 30 to 40 Torr of He. They used numerical simulations to obtain the HCl yield and report a value of (6.6 ± 3.5)% at 297 K. Lipson et al.[6] used a discharge-turbulent flow reactor with CIMS detection to follow HCl production from reaction 1. They then used computer modeling to extract a value for k_{1b} and report an HCl yield of (7 ± 3)% which is independent of pressure between 94 and 203 Torr and independent of temperature between 207 and 298 K. These results agree with their previous measurement of a (5 ± 2)% DCl yield from OD + ClO.[7] Poulet et al.[8] used mass spectrometry to detect HCl from OH + ClO and Cl + HO_2. They then used modeling to determine k_{1a} and k_{1b} and report a value of k_{1a}/k_1 of (98 ± 12)% at 298 K. Earlier studies[9−11] obtained values for k_{1a}/k_1 by monitoring the increase in HO_2 and the loss of OH by using resonance fluorescence or laser magnetic resonance; HCl yields listed in the table are obtained by subtracting the reported k_{1a}/k_1 values from unity.

The agreement among the present study and the results of Tyndall et al.[5] and Lipson et al.[6] is good. These three studies, using very different experimental techniques and methods of data analysis, show that there is a significant HCl yield from reaction 1. Because the present results rely solely on a measured concentration ratio to obtain the yield, they are entirely independent of the value of k_1. One of the methods used by Hills and Howard[10] is also independent of k_1. All of the other determinations use numerical modeling or analysis methods to obtain HCl yields from experimental data. These results will depend to a greater or lesser degree on the value of k_1 and other rate constants used in the model or analysis. Lipson et al.[6] did a sensitivity test by changing k_1 by 50% and report only a 15% change in k_{1b}.

Reactant Internal Energy. The Cl + O_3 reaction (eq 2) used to form ClO is exothermic by 38.6 kcal $mole^{-1}$. This is sufficient to produce excited-state product ClO or O_2. A recent study[37] found that reaction 2 generated ClO radicals in the ground electronic state but in excited vibrational levels up to $v = 6$ with a maximum population at $v = 3$; rotational excitation was also observed. This same study found a vibrational quenching rate constant of 2×10^{-13} cm^3 $molecule^{-1}$ s^{-1} for N_2. Conversion of O_3 to ClO by reaction 2 has been observed to be less than 1 to 1 both in excess Cl[38] and in excess O_3.[14] Reactions

TABLE 4: Summary of HCl Yield Measurements

k_{1b}/k_1 (%)[a]	P (Torr)	T (K)	method[c]	comments	value of k_1 used (cm^3 $molecule^{-1}$ s^{-1})	ref
< 35	1−3 He	298	DLF−RF	Observe amount of HO_2 produced per initial OH at a given reaction time	9.1×10^{-12}	11
16 ± 14	1.0−1.1 He	293	DLF-LMR	Observe changes in OH and HO_2 when ClO added	not needed	10
12 ± 10	1.0−1.1 He	293	DLF-LMR	Model OH and HO_2 vs time	1.8×10^{-11}	10
15 ± 18	1−5 He	243−298	DLF−RF	Observe changes in OH when add ClO and NO; use numerical model to extract k_{1a}/k_1	1.2×10^{-11}	9
2 ± 12[b]	0.7−0.9 He	298	DLF-LIF-EIMS	Observe HCl formation in excess O_3 and then excess Cl atoms; use numerical model to extract k_{1a} and k_{1b}	1.9×10^{-11}	8
5 ± 2 (DCl)	91−181 N_2	211−298	DTF−CIMS	Observe DCl formation vs time; use numerical model to extract k_{1b}	4.2×10^{-12} exp(280/T), 1.1×10^{-11} at 298 K	7
7 ± 3	94−203 N_2	207−298	DTF−CIMS	Observe HCl formation vs time; use numerical model to extract k_{1b}	5.5×10^{-12} exp(292/T), 1.5×10^{-11} at 298 K	6
6.6 ± 3.5	30−40 He	297	FP-LPIR	Observe HCl formation vs time; use numerical model to obtain yield	1.9×10^{-11}	5
9.0 ± 4.8	1.0 He	218−298	DLF−RF LPIR−UVA	Observe amount of HCl produced per OH consumed	not needed	present study

[a] Unless otherwise noted, uncertainties are two standard deviations plus estimated systematic errors. [b] One standard deviation plus estimated systematic errors. [c] CIMS = chemical ionization mass spectrometry; DLF = discharge laminar flow; DTF = discharge turbulent flow; EIMS = electron impact mass spectrometry; FP = flash photolysis; LIF = laser induced fluorescence; LMR = laser magnetic resonance; LPIR = long-path infrared spectrometry; RF = resonance fluorescence; UVA = ultraviolet absorption spectrometry.

(eqs 17 and 18) of excited ClO have been suggested[39] to account for these observations.

$$ClO^* + O_3 \rightarrow ClO + O_2 + O \quad (17)$$

$$ClO^* + Cl \rightarrow Cl_2 + O \quad (18)$$

Because we monitor ClO after the Cl + O_3 reaction is completed, possible nonstoichiometric conversion does not interfere with the ClO concentration measurements. Moreover, in our system there is an average delay of about 128 ms between the start of ClO formation and the start of the OH + ClO reaction. At total pressures of 1 Torr or more, this is sufficient time to deactivate any "hot" ClO either by gas-phase or wall quenching.

Although there is sufficient energy to produce electronically excited O_2 in the sigma ($^1\Sigma_g+$) and delta ($^1\Delta_g$) states, neither state has been observed as a product of reaction 2. Detection sensitivities and computer simulations have been used to estimate upper limits for the yields: < 0.05% for the sigma state and < 2.5% for delta.[39] Even if the delta state is formed at 2% yields, it is not expected to interfere with the present measurements because of its low reactivity.

The OH source reactions are also sufficiently exothermic to produce energy-rich products. The F + H_2O reaction (eq 7) releases 17.0 kcal mol^{-1} and can form vibrationally excited OH up to $v = 1$. The H + NO_2 reaction (eq 8) releases 29.1 kcal mol^{-1} and theoretically could form OH in vibrational states up to $v = 3$. Observed vibrational populations formed by this reaction are concentrated mostly up to $v = 2$, with a small fraction in $v = 3$.[40] The excited nascent OH can be deactivated by collisional or reactive quenching in the gas phase or at the walls. Deactivation rate constants have been measured for OH-($v = 1$) collisions with NO_2 and with H_2O; the reported values are 4.8×10^{-11} cm^3 $molecule^{-1}$ s^{-1} [41] and 1.4×10^{-11} cm^3 $molecule^{-1}$ s^{-1},[41,42] respectively. We can use this information to estimate the vibrational deactivation in both OH sources. In the H + NO_2 source, $[NO_2] \approx 2.5 \times 10^{13}$ molecules cm^{-3}; using the reported rate constant, we estimate the vibrationally excited OH should be reduced to less than 30% of its initial value within the source residence time of about 1 ms. In the F + H_2O source, $[H_2O] \approx 3 \times 10^{14}$ molecules cm^{-3}, and a similar estimate shows excited OH should be completely removed within the residence time of about 3 ms. Vibrational excitation of OH radicals could enhance the rate of the OH + H_2 reaction (eq 19), but the H atoms formed would be quickly converted back to OH by the excess NO_2 in the reactor.

$$OH + H_2 \rightarrow H_2O + H \quad (19)$$

Vibrational excitation of OH should reduce the importance of the third-order recombination (eq 20) with NO_2 but could enhance the second-order reaction (eq 21) which can become exothermic if OH is vibrationally excited.

$$OH + NO_2 + He \rightarrow HONO_2 + He \quad (20)$$

$$OH + NO_2 \rightarrow HO_2 + NO \quad (21)$$

The HO_2 formed could remove some OH or react with NO to produce OH again. Because vibrationally excited OH is essentially gone before the OH concentration is measured and the OH + ClO reaction begins, we conclude that reactions of excited OH are not important in our system. Moreover, there is no significant variation in the observed HCl yield using two very different OH sources. The difference in the initial vibrational distributions and quenching rates is additional evidence that excited OH did not interfere with the present measurements.

Comparison with Theory. Calculations using RRKM and statistical models[2,6] have shown that reaction 1 proceeds by an addition mechanism to form an excited HOOCl complex. The reaction can then proceed by four processes: (1) redissociation of the complex to reactants; (2) formation of Cl + HO_2 products; (3) formation of a four-center transition state (about 2 kcal mol^{-1}

below the reactants) with subsequent elimination of HCl + O_2; and (4) complex stabilization. Competition among the latter three processes determines the HCl yield. The theories predict HCl yields in the range observed experimentally. Also in agreement with experiment, theories predict only small dependencies on temperature and pressure. The calculations also show that the excited complex is not stabilized under atmospheric or laboratory conditions. Another theoretical study[43] places the four-center transition state at energies higher than the reactants. Although HCl yields were not calculated, the higher energy would be consistent with yields that could be lower than those calculated by the earlier studies.[2,6]

Wall Reaction. The flow reactor is designed to minimize wall reactions by using a low surface-to-volume ratio and by coating all surfaces in contact with reactive species with halocarbon wax which is well known to reduce surface reaction. In addition, the walls are conditioned by exposing them to OH radicals for several hours prior to each series of experimental runs. As seen in Table 2, the OH wall losses are about 10 s^{-1} at room temperature and show no large increase down to 258 K. OH wall losses at lower temperatures down to 218 K have also been measured[44] and are generally less than 10 s^{-1}. The low reactivity of the coated surfaces suggests that wall reaction is not a significant source of HCl in the present study. This is supported by the fact that the observed HCl yields are independent of temperature because one would expect surface reactions to become evident as the temperature is changed over a wide range.

Nonlinear OH Lamp Response at High Concentrations. As shown in Figure 3b, the OH lamp response is linear in [OH] up to about 3×10^{12} molecules cm^{-3}. Since $[OH]_o$ ranged up to about 6×10^{12} in some of the yield measurements, the possible effect of this nonlinearity needs to be addressed. The response of the HCl detection system was linear at least up to 8×10^{11} molecules cm^{-3} and most of the measurements were well within the linear region. For each experimental determination, the HCl yield is obtained by extrapolating a linear least-squares fit of the observed yield vs $[OH]_o$ to zero. To test for possible effects of the nonlinear OH response, the yields were recalculated by the same extrapolation procedure after excluding all data points for which $[OH]_o \geq 3 \times 10^{12}$ molecules cm^{-3}. The results agree with those using data over the entire range of $[OH]_o$; the agreement is within one standard deviation for all of the runs except two, and for these within two standard deviations. The overall average excluding runs for which $[OH]_o \geq 3 \times 10^{12}$ molecules cm^{-3} is 9.4 ± 6.8% compared to 9.0 ± 4.8% when all $[OH]_o$ are used. This small change shows that any nonlinearity in OH response had no significant effect on the results.

Acknowledgment. The research described in this article was performed at the Jet Propulsion Laboratory, California Institute of Technology, under a contract with the National Aeronautics and Space Administration. We thank G. S. Tyndall for communicating the HCl yield results prior to publication.

References and Notes

(1) Chance, K.; Traub, W. A.; Johnson, D. G.; Jucks, K. W.; Ciarpallini, P.; Stachnik, R. A.; Salawitch, R. J.; Michelsen, H. A. *J. Geophys. Res.* **1996**, *101*, 9031.

(2) Dubey, M. K.; McGrath, M. P.; Smith, G. P.; Rowland, F. S. *J. Phys. Chem. A* **1998**, *102*, 3127.

(3) Sen, B.; Osterman, G. B.; Salawitch, R. J.; Toon, G. C.; Margitan, J. J.; Blavier, J. F.; Chang, A. Y.; May, R. D.; Webster, C. R.; Stimpfle, R. M.; Bonne, G. P.; Voss, P. B.; Perkins, K. K.; Anderson, J. G.; Cohen, R. C.; Elkins, J. W.; Dutton, G. S.; Hurst, D. F.; Romashkin, P. A.; Atlas, E. L.; Schauffler, S. M.; Loewenstein, M. *J. Geophys. Res. Atmos.* **1999**, *104*, 26653.

(4) Ricaud, P.; Chipperfield, M. P.; Waters, J. W.; Russell, J. M.; Roche, A. E. *J. Geophys. Res. Atmos.* **2000**, *105*, 4459.

(5) Tyndall, G. S.; Kegley-Owen, C. S.; Orlando, J. J.; Fried, A. *J. Phys. Chem.* **2001**, to be submitted.

(6) Lipson, J. B.; Beiderhase, T. W.; Molina, L. T.; Molina, M. J.; Olzmann, M. *J. Phys. Chem. A* **1999**, *103*, 6540.

(7) Lipson, J. B.; Elrod, M. J.; Beiderhase, T. W.; Molina, L. T.; Molina, M. J. *J. Chem. Soc., Faraday Trans.* **1997**, *93*, 2665.

(8) Poulet, G.; Laverdet, G.; Le Bras, G. *J. Phys. Chem.* **1986**, *90*, 159.

(9) Burrows, J. P.; Wallington, T. J.; Wayne, R. P. *J. Chem. Soc., Faraday Trans. 2* **1984**, *80*, 957.

(10) Hills, A. J.; Howard, C. J. *J. Chem. Phys.* **1984**, *81*, 4458.

(11) Leu, M. T.; Lin, C. L. *Geophys. Res. Lett.* **1979**, *6*, 425.

(12) Wang, J. J.; Keyser, L. F. *J. Phys. Chem. A* **1999**, *103*, 7460.

(13) Sander, S. P.; Friedl, R. R.; DeMore, W. B.; Ravishankara, A. R.; Golden, D. M.; Kolb, C. E.; Kurylo, M. J.; Hampson, R. F.; Huie, R. E.; Molina, M. J.; Moortgat, G. K. *Chemical Kinetics and Photochemical Data for Use in Stratospheric Modeling, Evaluation No. 13;* Jet Propulsion Laboratory, California Institute of Technology: Pasadena, CA, 2000; JPL Publication 00-3.

(14) Kegley-Owen, C. S.; Gilles, M. K.; Burkholder, J. B.; Ravishankara, A. R. *J. Phys. Chem. A* **1999**, *103*, 5040.

(15) Trolier, M.; Mauldin, R. L., III; Ravishankara, A. R. *J. Phys. Chem.* **1990**, *94*, 4896.

(16) Simon, F. G.; Schneider, W.; Moortgat, G. K.; Burrows, J. P. *J. Photochem. Photobiol. A: Chem.* **1990**, *55*, 1.

(17) Sander, S. P.; Friedl, R. R. *J. Phys. Chem.* **1989**, *93*, 4764.

(18) Mandelman, M.; Nicholls, R. W. *J. Quant. Spectrosc. Radiat. Transfer* **1977**, *17*, 483.

(19) Johnston, H. S.; Morris, E. D., Jr.; Van den Bogaerde, J. *J. Am. Chem. Soc.* **1969**, *91*, 7712.

(20) Molina, L. T.; Molina, M. J. *J. Geophys. Res.* **1986**, *91*, 14501.

(21) DeMore, W. B.; Sander, S. P.; Howard, C. J.; Ravishankara, A. R.; Golden, D. M.; Kolb, C. E.; Hampson, R. F.; Kurylo, M. J.; Molina, M. J. *Chemical Kinetics and Photochemical Data for Use in Stratospheric Modeling, Evaluation No. 12;* Jet Propulsion Laboratory, California Institute of Technology: Pasadena, CA, 1997; JPL Publication 97-4.

(22) Lee, Y.-P.; Stimpfle, R. M.; Perry, R. A.; Mucha, J. A.; Evenson, K. M.; Jennings, D. A.; Howard, C. J. *Int. J. Chem. Kinet.* **1982**, *14*, 711.

(23) Altmann, J.; Baumgart, R.; Weitkamp, C. *Appl. Optics* **1981**, *20*, 995.

(24) Herriott, D.; Kogelnik, H.; Kompfner, R. *Appl. Optics* **1964**, *3*, 523.

(25) HITRAN−PC, *Database of Atmospheric Spectral Lines*, University of South Florida, 1992.

(26) Braun, W.; Herron, J. T.; Kahaner, D. K. *Int. J. Chem. Kinet.* **1988**, *20*, 51.

(27) IBM, CKS *Chemical Kinetics Simulator*, IBM Almaden Research Center; IBM Corporation 1995 (Internet address is http://www.almaden.ibm.com/st/msim/).

(28) Mallard, W. G.; Westley, F.; Herron, J. T.; Hampson, R. F.; Frizzell, D. H. *NIST Chemical Kinetics Data Base* **1998**, Version 2Q98.

(29) Knight, G. P.; Beiderhase, T.; Helleis, F.; Moortgat, G. K., Crowley, J. N. *J. Phys. Chem. A* **2000**, *104*, 1674.

(30) Finkbeiner, M.; Crowley, J. N.; Horie, O.; Müller, R.; Moortgat, G. K.; Crutzen, P. J. *J. Phys. Chem.* **1995**, *99*, 16264.

(31) Burrows, J. P.; Cox, R. A. *J. Chem. Soc., Faraday Trans. 1* **1981**, *77*, 2465.

(32) Leu, M.-T *Geophys. Res. Lett.* **1980**, *7*, 173.

(33) Leck, T. J.; Cook, J. E. L.; Birks, J. W. *J. Chem. Phys.* **1980**, *72*, 2364.

(34) Cattell, F. C.; Cox, R. A. *J. Chem. Soc., Faraday Trans. 2* **1986**, *82*, 1413.

(35) Lee, Y.-P.; Howard, C. J. *J. Chem. Phys.* **1982**, *77*, 756.

(36) Burrows, J. P.; Cliff, D. I.; Harris, G. W.; Thrush, B. A.; Wilkinson, J. P. T. *Proc. R. Soc. London* **1979**, *A368*, 463.

(37) Baumgärtel, S.; Delmdahl, R. F.; Gericke, K. H.; Tribukait, A. *Eur. Phys. J. D* **1998**, *4*, 199.

(38) Burkholder, J. B.; Hammer, P. D.; Howard, C. J.; Goldman, A. *J. Geophys. Res.* **1989**, *94*, 2225.

(39) Choo, K. Y.; Leu, M.-T *J. Phys. Chem.* **1985**, *89*, 4832.

(40) Irvine, A. M. L.; Smith, I. W. M.; Tuckett, R. P.; Yang, X.-F. *J. Chem. Phys.* **1990**, *93*, 3177 and earlier references cited herein.

(41) Smith, I. W. M.; Williams, M. D. *J. Chem. Soc., Faraday Trans. 2* **1985**, *81*, 1849.

(42) Glass, G. P.; Endo, H.; Chaturvedi, B. K. *J. Chem. Phys.* **1982**, *77*, 5450.

(43) Sumathi, R.; Peyerimhoff, S. D. *Phys. Chem. Chem. Phys.* **1999**, *1*, 5429.

(44) Wang, J. J.; Keyser, L. F. *J. Phys. Chem.* **2001**, to be submitted.